

Title	Undoped Layered Perovskite Oxynitride Li _{1-x} LaTa _{1-x} O ₃ N for Photocatalytic CO ₂ Reduction with Visible Light
Author(s)	Oshima, Takayoshi; Ichibha, Tom; Qin, Ken Sinkou; Muraoka, Kanemichi; Vequizo, Junie Jhon M.; Hibino, Keisuke; Kuriki, Ryo; Yamashita, Shunsuke; Hongo, Kenta; Uchiyama, Tomoki; Fujii, Kotaro; Lu, Daling; Maezono, Ryo; Yamakata, Akira; Kato, Hideki; Kimoto, Koji; Yashima, Masatomo; Uchimoto, Yoshiharu; Kakihana, Masato; Ishitani, Osamu; Kageyama, Hiroshi; Maeda, Kazuhiko
Citation	Angewandte Chemie International Edition (2018), 57(27): 8154-8158
Issue Date	2018-07-02
URL	http://hdl.handle.net/2433/232711
Right	© 2018 The Authors. Published by Wiley-VCH Verlag GmbH & Co. KGaA. This is an open access article under the terms of the Creative Commons Attribution-NonCommercial License, which permits use, distribution and reproduction in any medium, provided the original work is properly cited and is not used for commercial purposes.
Type	Journal Article
Textversion	publisher

Perovskites

International Edition: DOI: 10.1002/anie.201803931

German Edition: DOI: 10.1002/ange.201803931

Undoped Layered Perovskite Oxynitride $\text{Li}_2\text{LaTa}_2\text{O}_6\text{N}$ for Photocatalytic CO_2 Reduction with Visible Light

Takayoshi Oshima, Tom Ichibha, Ken Sinkou Qin, Kanemichi Muraoka, Junie Jhon M. Vequizo, Keisuke Hibino, Ryo Kuriki, Shunsuke Yamashita, Kenta Hongo, Tomoki Uchiyama, Kotaro Fujii, Daling Lu, Ryo Maezono, Akira Yamakata, Hideki Kato, Koji Kimoto, Masatomo Yashima, Yoshiharu Uchimoto, Masato Kakihana, Osamu Ishitani, Hiroshi Kageyama, and Kazuhiko Maeda*

Abstract: Oxynitrides are promising visible-light-responsive photocatalysts, but their structures are almost confined with three-dimensional (3D) structures such as perovskites. A phase-pure $\text{Li}_2\text{LaTa}_2\text{O}_6\text{N}$ with a layered perovskite structure was successfully prepared by thermal ammonolysis of a lithium-rich oxide precursor. $\text{Li}_2\text{LaTa}_2\text{O}_6\text{N}$ exhibited high crystallinity and visible-light absorption up to 500 nm. As opposed to well-known 3D oxynitride perovskites, $\text{Li}_2\text{LaTa}_2\text{O}_6\text{N}$ supported by a binuclear Ru^{II} complex was capable of stably and selectively converting CO_2 into formate under visible light ($\lambda > 400$ nm). Transient absorption spectroscopy indicated that, as compared to 3D oxynitrides, $\text{Li}_2\text{LaTa}_2\text{O}_6\text{N}$ possesses a lower density of mid-gap states that work as recombination centers of photogenerated electron/hole pairs, but a higher density of reactive electrons, which is responsible for the higher photocatalytic performance of this layered oxynitride.

Semiconductor materials that can split water into H_2 and O_2 as photocatalysts have been extensively explored and developed.^[1] Recently, the research interest is being expanded to CO_2 reduction, but it is generally very difficult to achieve the reaction because of the lack of active sites for CO_2 reduction on the surface as well as the predominant occurrence of competitive H_2 evolution reaction.^[2] Some layered perovskite oxides consisting of Ti^{4+} , Nb^{5+} , and Ta^{5+} have been regarded as high-potential photocatalysts for water splitting and CO_2 reduction.^[3,4]

Since most of metal oxide photocatalysts have large band gaps (> 3 eV) and are hence inactive under visible light ($\lambda > 400$ nm),^[5] mixed-anion compounds such as oxynitrides have attracted considerable attention as potential visible-light-responsive photocatalysts toward solar energy conversion.^[6,7] While nitrogen-doping into oxides is a conventional and facile

[*] T. Oshima, K. Muraoka, K. Hibino, R. Kuriki, Prof. Dr. K. Fujii, Prof. Dr. M. Yashima, Prof. Dr. O. Ishitani, Prof. Dr. K. Maeda
Department of Chemistry, School of Science
Tokyo Institute of Technology
2-12-1-NE-2 Ookayama, Meguro-ku, Tokyo 152-8550 (Japan)
E-mail: maedak@chem.titech.ac.jp

T. Oshima, K. Muraoka, R. Kuriki
Japan Society for the Promotion of Science
Kojimachi Business Center Building
5-3-1 Kojimachi, Chiyoda-ku, Tokyo 102-0083 (Japan)

T. Ichibha, K. S. Qin, Prof. Dr. R. Maezono
School of Information Science, JAIST
Asahidai 1-1, Nomi, Ishikawa 923-1292 (Japan)

Dr. J. J. M. Vequizo, Prof. Dr. A. Yamakata
Graduate School of Engineering, Toyota Technological Institute
2-12-1 Hisakata, Tempaku, Nagoya 468-8511 (Japan)

Dr. S. Yamashita, Dr. K. Kimoto
Research Center for Advanced Measurement and Characterization
National Institute for Materials Science
1-1 Namiki, Tsukuba, Ibaraki 305-0044 (Japan)

Prof. Dr. K. Hongo
Research Center for Advanced Computing Infrastructure, JAIST
Asahidai 1-1, Nomi, Ishikawa 923-1292 (Japan)

and
Center for Materials Research by Information Integration, Research and Services Division of Materials Data and Integrated System,
National Institute for Materials Science
Tsukuba 305-0047 (Japan),

and
PRESTO (Japan) Science and Technology Agency
4-1-8 Honcho, Kawaguchi-shi, Saitama 322-0012 (Japan)



Prof. Dr. K. Hongo, Prof. Dr. R. Maezono
Computational Engineering Applications Unit, RIKEN
2-1 Hirosawa, Wako, Saitama 351-0198 (Japan)


Dr. T. Uchiyama, Prof. Dr. Y. Uchimoto
Graduate school of Human and Environmental Studies
Kyoto University
Yoshida-nihonmatsu-cho, Sakyo-ku, Kyoto 606-8501 (Japan)

Dr. D. Lu
Suzukakedai Materials Analysis Division
Technical Department, Tokyo Institute of Technology
4259 Nagatsuta-cho, Midori-ku, Yokohama 226-8503 (Japan)

Prof. Dr. H. Kato, Prof. Dr. M. Kakihana
Institute of Multidisciplinary Research for Advanced Materials
Tohoku University
2-1-1 Katahira, Aoba-ku, Sendai 980-8577 (Japan)

Prof. Dr. H. Kageyama
Graduate School of Engineering, Kyoto University
Nishikyo-ku, Kyoto 615-8510 (Japan)

 Supporting information and the ORCID identification number(s) for the author(s) of this article can be found under:
 <https://doi.org/10.1002/anie.201803931>.

 © 2018 The Authors. Published by Wiley-VCH Verlag GmbH & Co. KGaA. This is an open access article under the terms of the Creative Commons Attribution-NonCommercial License, which permits use, distribution and reproduction in any medium, provided the original work is properly cited and is not used for commercial purposes.

method to induce visible light response,^[8] the charge imbalance between oxide and nitride anions (O^{2-} vs. N^{3-}) inevitably introduces defect states, which act as recombination centers of photoexcited carriers, and lower photocatalytic activity as seen in nitrogen-doped TiO_2 .^[9] Furthermore, the limited amount of doped nitrogen results in insufficient visible light absorption.

Undoped oxynitrides are therefore highly desirable. One such example is a three-dimensional (3D) perovskite oxynitride $CaTaO_2N$ (Figure 1 left), which can serve as an

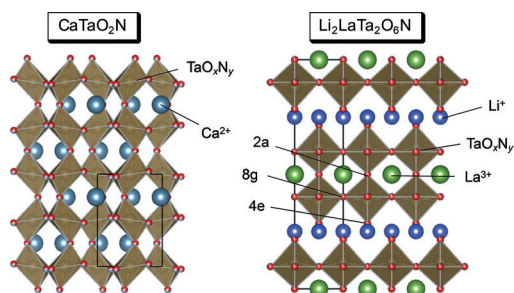


Figure 1. Crystal structures of $CaTaO_2N$ (left) and $Li_2LaTa_2O_6N$ (right) with Wyckoff positions of anion sites. The black solid squares indicate unit cells.

effective semiconductor component in a photocatalytic CO_2 reduction system, with the aid of a binuclear Ru^{II} complex (**RuRu'**; Supporting Information, Figure S1).^[10] The combined system, **RuRu'**/semiconductor, works as follows; both semiconductor and metal complex are excited by visible light. Holes in the valence band of the semiconductor oxidize an electron donor and the electron in conduction band reductively quenches the excited state of the photosensitizer unit of **RuRu'**, producing one electron reduced species (OERS) of the photosensitizer unit. Electron transfer occurs from the OERS to the catalyst moiety, finally reducing CO_2 (Supporting Information, Figure S2).^[11] In this hybrid system, low efficiencies of semiconductors and metal complexes for reduction and oxidation reactions can be addressed by utilizing efficient CO_2 reduction ability of metal complexes and strong oxidation ability of semiconductors, respectively.

Two-dimensional (2D) layered oxynitrides may improve the catalytic performance under visible light, but synthesis of layered oxynitrides is generally difficult. There are so far only a few reports of undoped layered oxynitrides (for example, Ba_2TaO_3N , $Rb_{1.8}LaNb_2O_{6.3}N_{0.7} \cdot 1.0H_2O$, and $K_{1.6}Ca_2Nb_3O_{9.4}N_{0.6} \cdot 1.1H_2O$),^[12,13] but accompanied with byproduction of thermally stable 3D perovskite phases in some cases. Additionally, photocatalytic performance of these undoped layered oxynitrides has not been investigated in detail.

Herein we demonstrate that a 2D layered oxynitride $Li_2LaTa_2O_6N$, composed of double-layer $[LaTa_2O_6N]^{2-}$ perovskite slabs that are separated by two Li cations (Figure 1 right), is a promising visible-light photocatalyst. This material was originally prepared by Fukuda et al.,^[13] but together with $LaTaON_2$ as a byproduct. Furthermore, photophysical and photocatalytic properties of $Li_2LaTa_2O_6N$ remain unexplored. Herein, we report the synthesis of a phase-pure $Li_2LaTa_2O_6N$.

The photocatalytic activities for CO_2 reduction under visible light irradiation ($\lambda > 400$ nm) were discussed, particularly in comparison with 3D perovskite analogues (that is, $LaTaON_2$ and $CaTaO_2N$).

$Li_2LaTa_2O_6N$ was synthesized by high-temperature ammonolysis using an amorphous oxide precursor containing Li, La, and Ta. The precursor was prepared by the polymerized complex method developed by Kakihana,^[14] a method that allows metal cations in a metal oxide to disperse homogeneously. Large efforts were devoted to identify the synthesis conditions to reduce the quantity of the byproducts. Various parameters (for example, reaction temperature, duration, and NH_3 flow rate) need to be optimized (1173 K, 12 h, and 20 mL min^{-1} of NH_3 flow); otherwise both $LaTaON_2$ and $LiTaO_3$ were readily formed (Supporting Information, Figure S3).

We also found that inclusion of an excess amount of Li in the oxide precursor is critical (Supporting Information, Figure S4). Nitridation of a stoichiometric precursor (0% excess Li) resulted in byproduct formation such as $LaTaON_2$, which is consistent with the previous work.^[13] Adding 10% excess of Li resulted in a single-phase $Li_2LaTa_2O_6N$. Further addition of Li (20%) yielded other diffraction peaks assignable to $LiTaO_3$. Because alkali metal species in oxide precursors usually are prone to volatilization at high temperatures,^[4] it is likely that the use of excess amount of Li compensated the loss during the high temperature ammonolysis. Unless stated otherwise, when we hereafter address $Li_2LaTa_2O_6N$, it means the one prepared with 10% excess of Li.

We checked the crystal structure of $Li_2LaTa_2O_6N$ using the Rietveld analysis of the X-ray powder diffraction data (Supporting Information, Figure S5), assuming the tetragonal ($I4/mmm$) layered perovskite structure (Figure 1).^[13] The refined lattice parameters were $a, b = 3.9533(4) \text{ \AA}$ and $c = 18.452(3) \text{ \AA}$, with reasonable reliability factors of $R_{wp} = 0.1076$, $R_B = 0.0623$, and $R_F = 0.0447$. Note that the small contrast in X-ray scattering between O and N did not allow us to examine the preference at the three anionic sites. We measured neutron diffraction, but could not obtain sufficient data because of high background.^[15]

Quantitative analysis for heavier elements (that is, La and Ta) was carried out using energy-dispersive X-ray spectroscopy (EDS), which indicated that the ratio of La/Ta in the synthesized $Li_2LaTa_2O_6N$ was 0.49.^[16] The nitrogen content of $Li_2LaTa_2O_6N$, measured using an elemental analyzer, was determined to be 2.07 wt%. These values are fairly close to the ideal values of 0.5 (for the La/Ta molar ratio) and 2.2 wt% (for N), respectively. Furthermore, charge neutrality of this compound led us to (tentatively) conclude that its composition is $Li_2LaTa_2O_6N$.

A typical scanning electron microscopy (SEM) measurement of $Li_2LaTa_2O_6N$ showed rectangular plate-like particles with size of a few hundred nanometers were observed, reflecting a layered nature of the structure (Supporting Information, Figure S6). The specific surface area determined by N_2 adsorption at 77 K was $2.4 \text{ m}^2 \text{ g}^{-1}$.

We conducted scanning transmission electron microscopy (STEM) to obtain atomic-resolution images of $Li_2LaTa_2O_6N$. Figure 2a shows a typical high-angle annular dark-field

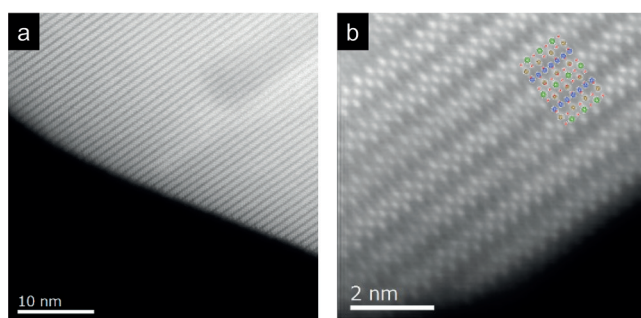


Figure 2. a) HAADF-STEM image and b) magnified HAADF-STEM image of $\text{Li}_2\text{LaTa}_2\text{O}_6\text{N}$ synthesized at 1173 K for 12 h under 20 mL min^{-1} of NH_3 flow. In (b), the crystal structure of $\text{Li}_2\text{LaTa}_2\text{O}_6\text{N}$ is added: Li^+ blue, La^{3+} green, Ta^{5+} brown, $\text{O}^{2-}/\text{N}^{3-}$ red.

(HAADF)-STEM image, indicating the formation of layered structure. As the signal intensity in HAADF imaging is approximately proportional to Z^2 (where Z is the atomic number),^[17] La and Ta atomic columns can be seen as bright dots and the arrangement of these bright dots agreed well with La and Ta atomic positions expected from the crystal structure of $\text{Li}_2\text{LaTa}_2\text{O}_6\text{N}$ (Figure 2b). The observed high crystallinity of $\text{Li}_2\text{LaTa}_2\text{O}_6\text{N}$ can be advantageous as a photocatalyst.

The yellow color of the as-synthesized $\text{Li}_2\text{LaTa}_2\text{O}_6\text{N}$ (see Figure 3a) manifests the ability of visible light absorption. Diffuse reflectance spectra (DRS) of $\text{Li}_2\text{LaTa}_2\text{O}_6\text{N}$ and its precursor oxide are shown in Figure 3b. The oxide precursor

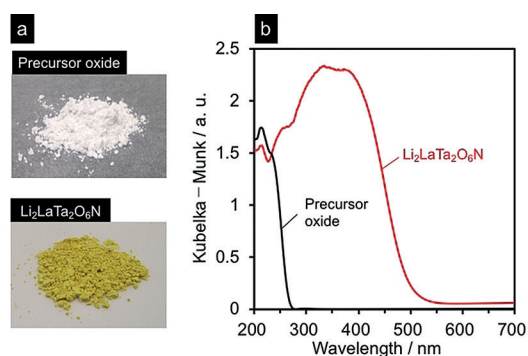


Figure 3. a) Photographs of the Li-La-Ta oxide precursor (top) and $\text{Li}_2\text{LaTa}_2\text{O}_6\text{N}$ (bottom). b) DRS of $\text{Li}_2\text{LaTa}_2\text{O}_6\text{N}$ and its precursor.

exhibited an absorption band only in UV light region, attributable to electron transfer from the valence band of O 2p orbitals to the conduction band formed by Ta 5d orbitals. The absorption band of $\text{Li}_2\text{LaTa}_2\text{O}_6\text{N}$ was extended to visible light region, with the band gap (estimated from the absorption edge) of ca. 2.5 eV. The red-shift strongly suggests the upward shift of the valence band owing to the inclusion of N 2p orbitals.

We measured the band-edge potentials of $\text{Li}_2\text{LaTa}_2\text{O}_6\text{N}$ by means of an electrochemical technique using a porous $\text{Li}_2\text{LaTa}_2\text{O}_6\text{N}$ electrode, which was prepared by an electrophoretic deposition method.^[18] Mott-Schottky plots (that is, capacitance⁻² (C^{-2}) vs. applied potential) of $\text{Li}_2\text{LaTa}_2\text{O}_6\text{N}$ with different frequencies are shown in the Supporting

Information, Figure S7. In all cases, the C^{-2} values decreased as the applied potential became more negative, a typical behavior for an n-type semiconductor. The flat-band potential of $\text{Li}_2\text{LaTa}_2\text{O}_6\text{N}$ was determined, from the potential at which the C^{-2} value is zero, to be $-1.75 \pm 0.13 \text{ V}$ (vs. Ag/AgNO_3). It is known that in an n-type semiconductor, the potential of the conduction band minimum is 0.1–0.3 V more negative than the flat-band potential.^[19] Owing to the uncertainty in conductivity of $\text{Li}_2\text{LaTa}_2\text{O}_6\text{N}$, we assumed the potential to be 0.2. The band structure of $\text{Li}_2\text{LaTa}_2\text{O}_6\text{N}$, along with LaTaON_2 and CaTaO_2N reported previously, are depicted in the Supporting Information, Figure S8.^[7,20] It can be seen that the conduction band potential of $\text{Li}_2\text{LaTa}_2\text{O}_6\text{N}$ is more negative than that of LaTaON_2 , but slightly more positive than CaTaO_2N . On the basis of physicochemical characterization demonstrated above, we conclude that $\text{Li}_2\text{LaTa}_2\text{O}_6\text{N}$ has a potential to serve as a photocatalyst under visible-light irradiation.

To clarify the origin of the new visible light absorption, density functional theory (DFT) calculations were performed. There are three different anionic sites, the bridging site (2a), the apical site (4e), and the equatorial site (8g). As we could not experimentally determine the nitrogen site in $\text{Li}_2\text{LaTa}_2\text{O}_6\text{N}$, we examined, for simplicity, three possibilities where nitride anions are selectively located at either 2a, 4e, or 8g site, and found that the structure with nitrogen at 8g gave the lowest energy, consistent with the Pauling's second rule.^[21]

The total and partial density of states of $\text{Li}_2\text{LaTa}_2\text{O}_6\text{N}$ in this configuration are shown in the Supporting Information, Figure S9a, where the conduction band was formed by Ta 5d orbital, while the middle-to-top of the valence band was occupied by a hybridized O 2p and N 2p orbital. In cases of 2a and 4e (Supporting Information, Figure S9b,c), the general feature found in the valence and conduction bands was almost the same, with only a small difference in the shape of the total DOS in the valence band. This means that regardless of the model, there is a significant contribution of N 2p orbital allowing the upward shift of the valence band maximum, responsible for the visible light absorption.

The result of UV/Vis diffuse reflectance spectroscopy and electrochemical measurements indicated that electron transfer from the conduction band of $\text{Li}_2\text{LaTa}_2\text{O}_6\text{N}$ (-1.95 V vs. Ag/AgNO_3) to the Ru photosensitizer unit ($+0.17 \text{ V}$) of **RuRu'** occurs as a thermodynamically favorable process. Thus, we applied the as-synthesized $\text{Li}_2\text{LaTa}_2\text{O}_6\text{N}$ for the CO_2 reduction system with the aid of **RuRu'**. The results of CO_2 reduction reactions are summarized in Table 1. After 15 h irradiation with a high-pressure mercury lamp ($\lambda > 400 \text{ nm}$), formate was detected as the major product with 97% selectivity, with only tiny amount of H_2 (entry 1). The turnover number (TON), which was defined as the ratio of the amount of formate generated to that of the adsorbed **RuRu'**, exceeded 50, confirming that the reaction took place catalytically. In the absence of either **RuRu'** (entry 2) or $\text{Li}_2\text{LaTa}_2\text{O}_6\text{N}$ (entry 3), no formate production was detected. Without irradiation, no reaction occurred (entry 4). It is notable that no significant change before and after the 15 h of reaction was observed in the XRD pattern and the light absorption profile of **RuRu'**/ $\text{Li}_2\text{LaTa}_2\text{O}_6\text{N}$ (Supporting Infor-

Table 1: Photocatalytic performance of CO₂ reduction over hybrid catalyst consisting of a semiconductor and RuRu' binuclear complex.^[a]

Entry	Photocatalyst	Products [nmol]		Selectivity to formate [%]
		Formate	H ₂	
1	RuRu'/Li ₂ LaTa ₂ O ₆ N	660	16	97
2	Li ₂ LaTa ₂ O ₆ N	N.D.	N.D.	–
3	RuRu'/Al ₂ O ₃	N.D.	N.D.	–
4 ^[b]	RuRu'/Li ₂ LaTa ₂ O ₆ N	N.D.	N.D.	–
5	RuRu'/Ag/Li ₂ LaTa ₂ O ₆ N	1440	16	99
6	RuRu'/CaTaO ₂ N	N.D.	N.D.	–
7	RuRu'/LaTaON ₂	N.D.	N.D.	–
8 ^[c]	RuRu'/Ag/CaTaO ₂ N	320	N.D.	> 99

[a] Reaction conditions: photocatalyst: 4.0 mg, reaction solution: a mixture of MeCN/TEOA (4:1 v/v) 4 mL; reaction vessel, Pyrex test tube with a septum (8 mL capacity); light source, 400 W high-pressure mercury lamp with a NaNO₂ solution filter. Reaction time: 15 h. In each case, RuRu' of 3 μmol g⁻¹ was adsorbed. ND = not detected. [b] Without irradiation. [c] In DMA/TEOA (4:1 v/v).

mation, Figure S10), indicating that Li₂LaTa₂O₆N is stable under the given reaction conditions.

It is necessary to check the carbon source of CO₂ reduction product(s) because some contaminated organic compounds on semiconductor surface may undergo unidentified photochemical processes to yield carbon-containing products.^[22] Thus, we initially performed CO₂ reduction under ¹³CO₂ atmosphere, and collected No-D ¹H-NMR spectra to verify the carbon source of formate. Unfortunately, the low activity/sensitivity of No-D NMR method did not allow the detection of any signal of products from RuRu'/Li₂LaTa₂O₆N. Accordingly, nanoparticulate Ag (1.5 wt%) was in prior deposited on Li₂LaTa₂O₆N to promote CO₂ reduction, as reported previously.^[10,11] Deposition of metallic Ag nanoparticles with 20–30 nm in size on Li₂LaTa₂O₆N was confirmed by means of XAFS and TEM observations (Supporting Information, Figures S11 and S12). This modification improved the formate production rate (entry 5, Table 1). After 15 h irradiation, a clear doublet signal ($J^{13}_{\text{CH}} = 174$ Hz) assignable to ¹³C of formate^[10,11] was observed between 8.54 and 8.05 ppm in the ¹H-NMR spectrum, while only singlet signal derived from H¹²COOH appeared when ¹²CO₂ was used (Supporting Information, Figure S13). The present results provide firm evidence that RuRu'/Ag/Li₂LaTa₂O₆N reduced CO₂ to formate.

We also compared the photocatalytic activity of the present system with those of the CaTaO₂N and LaTaON₂ counterparts without any modification other than RuRu'.^[23] Interestingly, Li₂LaTa₂O₆N demonstrated by far the highest performance among them, as listed in Table 1. We previously reported that prior modification of CaTaO₂N with Ag nanoparticles improved the formate production in the visible-light Z-scheme CO₂ reduction with RuRu'.^[10] However, even without modification of Ag, the activity of RuRu'/Li₂LaTa₂O₆N was two-fold higher than that of the optimized RuRu'/Ag/CaTaO₂N (entry 8). These results clearly indicate great potentials of layered oxynitride materials as a photocatalyst.

To elucidate the origin of different photocatalytic activities between the 2D and 3D oxynitrides (Li₂LaTa₂O₆N,

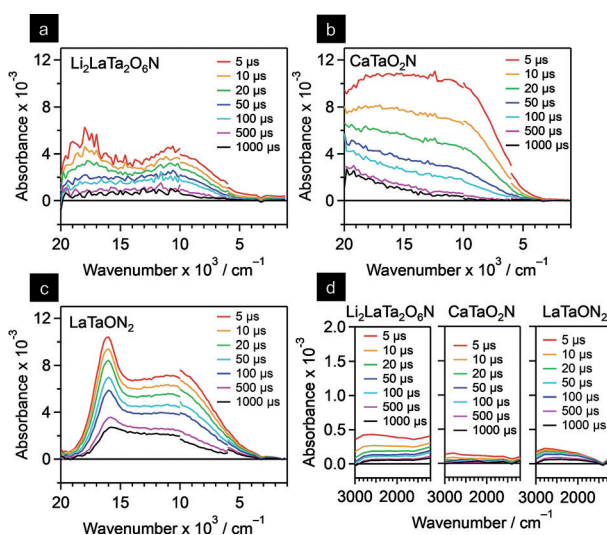


Figure 4. Transient absorption spectra for a) Li₂LaTa₂O₆N, b) CaTaO₂N, and c) LaTaON₂ recorded after 480 nm laser pulse excitation under vacuum. d) Enlarged views of each compound in the 3000–1200 cm⁻¹ region.

CaTaO₂N/LaTaON₂), transient absorption spectroscopy was applied to examine the nature of photogenerated charge carriers. Figure 4 shows transient absorption spectra of these oxynitrides after laser pulse excitation at 480 nm under vacuum. The laser excitation induced a broad absorption band over the range from 20000 to 1000 cm⁻¹. Here, the absorption from 20000 to 3000 cm⁻¹ is attributed to electrons/holes trapped at energetically deep defects,^[24] whereas that from 3000 to 1000 cm⁻¹ originates from shallowly trapped and/or free electrons. It is known that the shallowly trapped and/or free electrons are much more reactive and positively influence the photocatalytic activity than deeply trapped electrons. The shapes of the transient absorption spectra for these three materials were different. In particular, absorption bands attributed to the deeply trapped charges (20000–3000 cm⁻¹) in Li₂LaTa₂O₆N were weaker than those observed for CaTaO₂N and LaTaON₂. Furthermore, Li₂LaTa₂O₆N exhibited more pronounced signals from shallowly trapped and/or free electrons than CaTaO₂N and LaTaON₂. These observations could account for the higher photocatalytic activity of Li₂LaTa₂O₆N relative to CaTaO₂N and LaTaON₂: a larger portion of the photogenerated carriers in Li₂LaTa₂O₆N survived without undergoing recombination. We deduce that the 2D structure of Li₂LaTa₂O₆N as well as high crystallinity contributes to the unique photophysical property.

In conclusion, we synthesized a layered perovskite oxynitride of Li₂LaTa₂O₆N by thermal ammonolysis of a Li-La-Ta oxide precursor, and examined as a photocatalyst for visible-light CO₂ reduction in combination with a binuclear Ru^{II} complex (RuRu'). The production of single-phase Li₂LaTa₂O₆N was confirmed by means of XRD and HAADF-STEM measurements. The key to synthesize Li₂LaTa₂O₆N without producing impurity phases was the use of an oxide precursor that contained a proper (excess) amount of Li. The as-synthesized Li₂LaTa₂O₆N having a band

gap of about 2.5 eV, modified with **RuRu'**, was capable of photocatalyzing CO₂ reduction into formate under visible light ($\lambda > 400$ nm) with high selectivity (>97%), while analogues of 3D-type oxynitride perovskites of CaTaO₂N and LaTaON₂ were not. Transient absorption spectroscopy indicated that the lower density of trap states and higher density of reactive electrons were responsible for the high activity for CO₂ reduction.

Although known oxynitride photocatalysts are comprised of 3D-type materials, the result of the present study clearly demonstrates the high potential of a 2D layered oxynitride as a visible-light-driven photocatalyst. This is the first example of an undoped layered oxynitride that exhibits distinct photocatalytic activity, opening the possibility of new 2D layered oxynitride photocatalysts for artificial photosynthesis.

Acknowledgements

This work was supported by a Grant-in-Aid for Scientific Research on Innovative Area "Mixed Anion (Project JP16H06438, JP16H06439, JP16H06440, JP16H06441, JP17H05491, JP16K21724 and JP17H05478)" (JSPS). It was also partially supported by a Grant-in-Aids for Young Scientists (A) (Project JP16H06130), (B) (Project JP17K17762), for Fund for the Promotion of Joint International Research (Project JP16KK0097), a PRESTO program (Project JPMJPR16NA), and a CREST program (Project JPMJCR13L1) (JST). K.Ma. acknowledges The Noguchi Institute and Murata Research Foundation financial support. T.O., K.Mu., and R.K. wish to acknowledge support by a JSPS Fellowship for Young Scientists (JP16J10084, JP17J06914 and JP17J03705). K.Ho. is grateful to Support Program for Starting Up Innovation Hub MI²I from JST. The computations in this work have been performed using the facilities of the Center for Information Science in JAIST. R.M. is grateful for financial support from FLAGSHIP2020 (MEXT for the computational resources, Project Nos. hp170269 and hp180175 at K-computer), Toyota Motor Corporation, I-O DATA Foundation, and the Air Force Office of Scientific Research (AFOSR-AOARD/FA2386-17-1-4049).

Conflict of interest

The authors declare no conflict of interest.

Keywords: CO₂ reduction · oxynitride · perovskites · photocatalysis · visible light

How to cite: *Angew. Chem. Int. Ed.* **2018**, *57*, 8154–8158
Angew. Chem. **2018**, *130*, 8286–8290

- [1] A. Kudo, Y. Miseki, *Chem. Soc. Rev.* **2009**, *38*, 253–278.
- [2] a) K. Iizuka, T. Wato, Y. Miseki, K. Saito, A. Kudo, *J. Am. Chem. Soc.* **2011**, *133*, 20863–20868; b) K. Teramura, Z. Wang, S. Hosokawa, Y. Sakata, T. Tanaka, *Chem. Eur. J.* **2014**, *20*, 9906–9909.
- [3] T. Tanaka, K. Shinohara, A. Tanaka, M. Hara, J. N. Kondo, K. Domen, *J. Photochem. Photobiol. A* **1997**, *106*, 45–49.

- [4] K. Shimizu, S. Itoh, T. Hatamachi, T. Kodama, M. Sato, K. Toda, *Chem. Mater.* **2005**, *17*, 5161–5166.
- [5] D. E. Scaife, *Solar Energy* **1980**, *25*, 41–54.
- [6] a) G. Hitoki, T. Takata, J. N. Kondo, M. Hara, H. Kobayashi, K. Domen, *Chem. Commun.* **2002**, 1698–1699; b) K. Maeda, K. Teramura, D. Lu, T. Takata, N. Saito, Y. Inoue, K. Domen, *Nature* **2006**, *440*, 295; c) C. Pan, T. Takata, M. Nakabayashi, T. Matsumoto, N. Shibata, Y. Ikuhara, K. Domen, *Angew. Chem. Int. Ed.* **2015**, *54*, 2955–2959; *Angew. Chem.* **2015**, *127*, 2998–3002; d) H. Kageyama, K. Hayashi, K. Maeda, J. P. Atfield, Z. Hiroi, J. Rondinelli, K. R. Poeppelmeier, *Nat. Commun.* **2018**, *9*, 772.
- [7] H. Kato, K. Ueda, M. Kobayashi, M. Kakihana, *J. Mater. Chem. A* **2015**, *3*, 11824–11829.
- [8] a) G. Liu, L. Wang, C. Sun, X. Yan, X. Wang, Z. Chen, S. C. Smith, H. M. Cheng, G. Q. Lu, *Chem. Mater.* **2009**, *21*, 1266–1274; b) A. Mukherji, B. Seger, G. Q. Lu, L. Wang, *ACS Nano* **2011**, *5*, 3483–3492.
- [9] A. Nakada, S. Nishioka, J. J. M. Vequizo, K. Muraoka, T. Kanazawa, A. Yamakata, S. Nozawa, H. Kumagai, S. Adachi, O. Ishitani, K. Maeda, *J. Mater. Chem. A* **2017**, *5*, 11710–11719.
- [10] F. Yoshitomi, K. Sekizawa, K. Maeda, O. Ishitani, *ACS Appl. Mater. Interfaces* **2015**, *7*, 13092–13097.
- [11] K. Sekizawa, K. Maeda, K. Domen, K. Koike, O. Ishitani, *J. Am. Chem. Soc.* **2013**, *135*, 4596–4599.
- [12] a) S. J. Clarke, K. A. Hardstone, C. W. Michie, M. J. Rosseinsky, *Chem. Mater.* **2002**, *14*, 2664–2669; b) J. A. Schottenfeld, A. J. Benesi, P. W. Stephens, G. Chen, P. C. Eklund, T. E. Mallouk, *J. Solid State Chem.* **2005**, *178*, 2313–2321; c) A. da Silva Maia, F. Cheviré, V. Demange, V. Bouquet, M. Pasturel, S. Députier, R. Lebullenger, M. Guilloux-Viry, F. Tessier, *Solid State Sci.* **2016**, *54*, 17–21.
- [13] M. Kaga, H. Kurachi, T. Asaka, B. Yue, J. Ye, K. Fukuda, *Powder Diffr.* **2012**, *26*, 4–8.
- [14] M. Kakihana, *J. Sol-Gel Sci. Technol.* **1996**, *6*, 7–55.
- [15] Neutron powder diffraction data of Li₂LaTa₂O₆N was also measured at ANSTO in Australia (Proposal No. PP5198). However, the background probably due to the incoherent scattering of Li atom was too high to refine the precise crystal parameters.
- [16] We tried to quantify the concentration of Li in the synthesized Li₂LaTa₂O₆N by means of inductivity coupled plasma optical emission spectroscopy. However, the Li₂LaTa₂O₆N sample was not completely soluble in any of acid media we examined. Hence we could not determine the Li concentration at the present stage.
- [17] S. J. Pennycook, D. E. Jesson, *Ultramicroscopy* **1991**, *37*, 14–38.
- [18] R. Abe, M. Higashi, K. Domen, *J. Am. Chem. Soc.* **2010**, *132*, 11828–11829.
- [19] Y. Matsumoto, *J. Solid State Chem.* **1996**, *126*, 227–234.
- [20] S. Balaz, S. H. Porter, P. M. Woodward, L. J. Brillson, *Chem. Mater.* **2013**, *25*, 3337–3343.
- [21] F. Amparo, *Inorg. Chem.* **2006**, *45*, 9640–9642.
- [22] T. Yui, A. Kan, C. Saitoh, K. Koike, T. Ibusuki, O. Ishitani, *ACS Appl. Mater. Interfaces* **2011**, *3*, 2594–2600.
- [23] XRD and DRS measurements revealed that CaTaO₂N and LaTaON₂ were successfully synthesized without impurities via polymerized complex route (Supporting Information, Figure S14), and the band gaps were 2.5 and 2.0 eV, respectively, which are consistent with those reported in Refs. [7, 10].
- [24] A. Yamakata, M. Kawaguchi, N. Nishimura, T. Minegishi, J. Kubota, K. Domen, *J. Phys. Chem. C* **2014**, *118*, 23897–23906.

Manuscript received: April 2, 2018

Accepted manuscript online: May 8, 2018

Version of record online: May 30, 2018